J Neuropathol Exp Neurol
Vol. 77, No. 9, September 2018, pp. 803–813
doi: 10.1093/jnen/nly058

ORIGINAL ARTICLE

Blood Exposure Causes Ventricular Zone Disruption and Glial Activation In Vitro

Leandro Castaneyra-Ruiz, PhD, Diego M. Morales, MS, James P. McAllister, PhD, Steven L. Brody, MD, Albert M. Isaacs, MD, Jennifer M. Strahle, MD, Sonika M. Dahiya, MD, and David D. Limbrick, MD, PhD

Abstract

Intraventricular hemorrhage (IVH) is the most common cause of pediatric hydrocephalus in North America but remains poorly understood. Cell junction-mediated ventricular zone (VZ) disruption and astrogliosis are associated with the pathogenesis of congenital, nonhemorrhagic hydrocephalus. Recently, our group demonstrated that VZ disruption is also present in preterm infants with IVH. On the basis of this observation, we hypothesized that blood triggers the loss of VZ cell junction integrity and related cytopathology. In order to test this hypothesis, we developed an in vitro model of IVH by applying syngeneic blood to cultured VZ cells obtained from newborn mice. Following blood treatment, cells were assayed for N-cadherin-dependent adherens junctions, ciliated ependymal cells, and markers of glial activation using immunohistochemistry and immunoblotting. After 24–48 hours of exposure to blood, VZ cell junctions were disrupted as determined by a significant reduction in N-cadherin expression ($p < 0.05$). This was also associated with significant decrease in multiciliated cells and increase in glial fibrillary acid protein-expressing cells ($p < 0.05$). These observations suggest that, in vitro, blood triggers VZ cell loss and glial activation in a pattern that mirrors the cytopathology of human IVH and supports the relevance of this in vitro model to define injury mechanisms.

Key Words: Ependyma, Hydrocephalus, Intraventricular hemorrhage, N-cadherin, Ventricular zone.

INTRODUCTION

Intraventricular hemorrhage (IVH) remains the most frequent and severe neurological complication of premature birth, occurring in nearly 20% of preterm infants (1–3). Posthemorrhagic hydrocephalus (PHH) occurs in up to one-half of infants who develop IVH and now represents the most common cause of pediatric hydrocephalus in North America (4). Despite advances in neonatal and neurosurgical care, the neurological outcomes of infants with PHH remain among the worst in newborn medicine, with cognitive deficits in >85% of affected infants and cerebral palsy in 70% (1). PHH also requires complex, lifelong neurosurgical care (5–7) and frequently requires neurosurgical revision surgery, accounting for >$605 million in healthcare spending in the United States annually (4). Despite the high prevalence and poor outcomes in infants with PHH, the pathogenesis of this disorder remains poorly understood (8, 9).

It has been observed that the preterm ventricular zone (VZ) is altered in IVH (10). The preterm VZ is a single layer of monociliated neural stem cells (NSC) that develops into mature multiciliated ependymal cells (EC) to form a barrier separating the cerebrospinal fluid (CSF) from the brain parenchyma. The VZ and the subjacent subventricular zone are the primary sites of neurogenesis for the brain (11). NSC give rise to oligodendrocytes, astrocytes, and neurons, which use the radial basal processes of neighbor NSC as a scaffold for migration (11–14) and gliogenesis (15, 16). In humans, neurogenesis continues into the third trimester and newborn period (17), precisely when IVH and PHH commonly occur.

The cytopathology of the VZ following IVH has been characterized as an alteration in NSC/EC, with neuroepithelial injury, loss or detachment (VZ disruption), impaired cell junctions, and gliosis in the affected area. VZ disruption has been specifically implicated in the etiology of both congenital (nonhemorrhagic) hydrocephalus and PHH in both experimental models (17–25), and humans (26–31). Our group also reported that VZ disruption is a key feature in IVH in preterm human infants (10). More specifically, a cell-cell junction impairment or cell junction pathology appears to be involved in the origin of VZ disruption, since NSC/EC lose the capacity to attach to one another (22, 24, 25, 31, 32). In this setting, VZ disruption is characterized by altered N-cadherin (Cadherin2) adherens

From the Department of Neurological Surgery, Washington University School of Medicine and the St. Louis Children's Hospital, St. Louis, Missouri (LCR, DMM, JPM, JMS, DDL); Department of Medicine (SLB); Department of Neuroscience (AMI); Department of Pediatrics (JMS, DDL); and Department of Pathology & Immunology, Washington University School of Medicine, St. Louis, Missouri (SMD)

Send correspondence to: Leandro Castaneyra-Ruiz, PhD, Department of Neurological Surgery, Washington University School of Medicine, 660 South Euclid Ave., Campus Box 8057, St. Louis, MO 63110; E-mail: lcastan@wustl.edu

This study was supported by funding through NIH/NINDS K23 NS075151 (D.D.L.), the Children's Surgical Sciences Institute, St. Louis Children's Hospital (D.D.L.), and La Fundacion Canaria Dr Manuel Morales, 2016 (L.C.R).

The authors have no duality or conflicts of interest to declare.

Supplementary Data can be found at academic.oup.com/jnen.

junctions and connexin 43-dependent gap junctions, ependymal layer denudation, astrocytosis, and periventricular heterotopia (31). We hypothesized that this pathophysiology was the direct result of blood exposure in IVH. To test this hypothesis, we developed an EC culture model to determine the effects of blood exposure on temporal changes in VZ junctional integrity and associated markers of VZ cell injury.

MATERIALS AND METHODS

VZ Cell Cultures

All animal procedures were approved by the Institutional Animal Care and Use Committee (IACUC) of the Washington University School of Medicine. C57BL/6 mice at p 0 to 4 were used. Cells were dissociated with an enzymatic digestion solution (17 μL of Papain #37A17241, Worthington, Lakewood, NJ; 15 μL of DNAse, #EN0521, Thermo Fisher Scientific, Waltham, MA; and 288 μg of L-Cysteine, #C7352, Sigma, St. Louis, MO) in 1 mL of DMEM (Dulbecco's Modified Eagle Medium)/Glutamax per brain for 1 hour. Dissociated VZ cells were plated into 25 cm^2 flasks and grown in proliferation media composed of DMEM/Glutamax supplemented with 10% fetal bovine serum, 1% penicillin/streptomycin (P/S) at 37°C as described by Delgehyr et al (33). Half of the media was replaced the following day. After the cultures were confluent (~4 days), the flasks were shaken at 250 rpm overnight at room temperature to remove weakly attached cells, which were mainly differentiated neurons. The remaining cells were rinsed with Ca^{2+}/Mg^{2+}-free PBS (phosphate buffered saline) and incubated for 5 minutes at 37°C with 1 mL of trypsin-EDTA (ethylenediaminetetraacetic acid) to detach them from the flask. These cells were resuspended in proliferation media and replated onto 12-mm-diameter round glass coverslips in 24-well plates. The cell suspension (20 μL of 2×10^6 cells/mL) were carefully placed onto the coverslip and incubated for 1 hour, allowing the cells to adhere at high density, after which 1 mL of the proliferation media was added to each well. The following day, DMEM/Glutamax, 1% P/S (differentiation media) was used for continued culture; cells progressively differentiate from NSC to EC in this media (33).

Exposure of VZ Cultures to Blood

Five days after differentiation was initiated, the VZ cells were submerged in nonheparinized whole blood collected using orbital sinus puncture (34) from animals within the same colony. Blood samples were held at 4°C for <5 minutes. Cells on coverslips were treated with 25, 30, or 40 μL of blood for a total of 3, 24, or 48 hours in a pilot dose-response experiment and compared with control coverslips that were submerged in PBS under similar conditions. Subsequently, time-related experiments were performed comparing exposure of cells to 30 μL of PBS or blood for 3, 24, or 48 hours.

Immunocytochemistry

At 3, 24, and 48 hours after control PBS or blood treatment, the coverslips were washed 3 times with PBS and fixed with 4% paraformaldehyde in PBS for 7 minutes. After washing again in PBS, the cells were permeabilized with 5% bovine serum albumin in PBS and 1% Triton X-100 for 1 hour; subsequently the cells were incubated for 2 hours with antibodies diluted in PBS supplemented with 0.1% Triton X-100. Antibodies and dilutions included: N-cadherin (#180224, Thermo Fisher Scientific), 1:25; glial fibrillary acidic protein (GFAP) (#7260, Abcam, Cambridge, MA), 1:300; βIV tubulin (#11315, Abcam), 1:100; and active caspase-3 (#AF835, Novus Biologicals, Littleton, CO), 1:100. After rinsing 3 times with PBS, the coverslips were incubated for 1 hour with the appropriate secondary antibody, diluted in PBS supplemented with 0.1% Triton X-100: goat antimouse Alexa Fluor 488 (#A11001, Thermo Fisher Scientific), goat antirabbit Alexa Fluor 488 (#A11034, Invitrogen, Carlsbad, CA) at 1:300 or goat antimouse Alexa Fluor 555 (#AQ21422, Thermo Fisher Scientific) at 1:300. Lastly, the cells were stained with 4′ 6-diamidino-2-phenylindole (DAPI) at 1:5000 in PBS (#D1306, Thermo Fisher Scientific) for 5 minutes to label cell nuclei.

Western Blot

After 48 hours of PBS or blood treatment, the cells were rinsed with PBS until the remaining blood was removed and then treated with 50 μL of RIPA (radioimmunoprecipitation assay buffer) solution (#R0278 Sigma) to homogenize the cultures. Proteins were denatured in lithium dodecyl sulfate sample buffer (NP0007, Invitrogen, Carlsbad, CA) and reduced using β-mercaptoethanol (#M7154, Sigma). After heating at 95°C for 5 minutes, each 30 μL sample was run on an SDS-PAGE gel (4–12% polyacrylamide) (#NP0321, Invitrogen, Carlsbad, CA) for 1 hour at 120 V in SDS running buffer (#NP0001, Novex, Carlsbad, CA) and the proteins were then blotted onto a nitrocellulose membrane (#LC2006, Novex) at 170 mA for 2.5 hours in 15% Methanol transfer buffer (#NP0006, Novex). After blocking for 1 hour in Tris buffered saline with 5% powdered milk, samples were incubated with primary antibodies in Tris buffered saline (TBS) and 0.1% Tween at 4°C overnight. Primary antibodies and dilutions were GFAP (#7260, Abcam), 1:1000; N-cadherin (#180224, Thermo Fisher Scientific) 1:50 for and GAPDH (#2118S, Cell Signaling Technology, Danvers, MA), 1:500. Detection was performed by enhanced chemiluminescence (#7003, Cell Signaling Technology) after an hour of incubation with horseradish peroxidase-conjugated antirabbit, 1:10 000 (#70742, Cell Signaling Technology) or antimouse, 1:5000 (#SC-2005, Santa Cruz Biotechnology, Dallas, TX).

Image Analysis

Images of immunostained tissue were obtained using Pascal confocal microscopy at 20× (0.50 Zeiss, Oberkochen, Germany) and 63× (1.4 Zeiss). The NIH public software, ImageJ was used to quantify cell variations (total cells, number of cells expressing specific proteins, immunodensity). To calculate the total number of cells, an ImageJ macroinstruction was developed to quantify DAPI labeling (Supplementary Data Fig. S1) in areas of 0.0225 mm^2. Western blot images

were taken with the molecular imager *Chemidoc* XRS+ using *Image Lab* 3.0 from Bio-Rad (Hercules, CA).

Statistical Analysis

One-way ANOVA followed by the Tukey posthoc test or the Student *t*-test were used for parametric data and a Mann-Whitney *U* test was used for nonparametric data. Results were considered statistically significant if $p < 0.05$. Data are presented as group medians (nonparametric) or mean ± SD (parametric) and were considered statistically significant at $p < 0.05$. All analyses were conducted using Prism 5 (GraphPad Software, San Diego, CA).

RESULTS

In Vitro Development of EC

To define the normal development of EC in vitro, we used a previously described EC culture model in which the cells progressively differentiate from monociliated NSC to mature multiciliated EC. To evaluate differentiation, the cells were immunolabeled against the cilia marker βIV-tubulin, which allows us to discriminate between multiciliated, monociliated, and nonciliated VZ cells. To determine the stage of EC maturation, the glial marker GFAP was used; EC exhibit GFAP-positive attributes in premature stages and become GFAP-negative with maturation (10, 35–37). This approach permitted identification of 6 different cell types (Fig. 1): 1) cells not expressing GFAP or βIV-tubulin, 2) cells expressing GFAP but not βIV-tubulin, 3) monociliated βIV-tubulin cells not expressing GFAP, 4) monociliated βIV-tubulin cells expressing GFAP, 5) multiciliated βIV-tubulin cells expressing GFAP, and 6) multiciliated βIV-tubulin cells not expressing GFAP (Fig. 1D). In the current project, we focused on multiciliated EC.

Multiciliated EC developed from monociliated cells in a time-dependent fashion, comprising 3.73% ± 4.29%, 23.01% ± 7.56%, and 52.29% ± 11.07% ($p < 0.001$) of all viable cells at 3, 5, and 7 days after differentiation media was added (Fig. 1A, B). Overall, there was little change in the total number of cells at the same time points (day 3: 42.80 ± 7.64, day 5: 42.78 ± 8.61, day 7: 44.31 ± 6.87) after the initiation of differentiation, indicating that cells were changing from progenitor-like VZ cells to those that are typically found in the well-differentiated ependyma.

Double-labeling was performed against βIV-tubulin and GFAP at days 5 and 7, when a significant number of VZ cells had differentiated to EC (Fig. 1C, D). We found no significant increase in the percentage of GFAP-negative cells from among all multiciliated cells (day 5: 29.45 ± 18.84; day 7: 35.37 ± 33.77). At both time points, over 60% of the EC remained in a premature stage (still expressing GFAP); in addition, the total number of GFAP-positive cells did not change over time (day 5: 72.78 ± 9.42; day 7: 73.61 ± 12.47).

N-Cadherin-Dependent Cell Junctions in the Development of the VZ

Cell junction impairment is a hallmark in the initiation of the VZ disruption. We focused on N-cadherin as a dominant member of the cadherin adherens junction family. These intercellular junctions were detected in the membrane of all VZ cells, probably contributing to the characteristic polygonal shape that is permanent regardless of whether the cells were less differentiated (day 5) or more differentiated (day 7) EC (Fig. 1E). Interestingly, N-cadherin expression initially declined from day 5 to day 6 (respectively, 2.93 ± 2.41 vs 2.11 ± 2.03; $p > 0.05$) and then stabilized up to day 7 (2.22 ± 1.87), suggesting a possible heightened requirement for this cell junction protein during early stages of normal differentiation. Double-labeling with GFAP and N-cadherin showed that the polygonal shape existed independent of the expression of GFAP, indicating that GFAP may not affect the expression of N-cadherin. The glial projections of the GFAP-positive cells did not express N-cadherin (Fig. 1F).

Effects of Blood on VZ Disruption

To examine if blood exposure elicits NSC/EC loss, cell junction pathology, or astroglial response, VZ cultures at day 5 of differentiation were exposed to syngeneic blood and the effects were evaluated over time. The amount of blood needed for this model was determined in pilot experiments using 25 (2.5%), 30 (3%), and 40 μL (4%). After 3 hours of 40 μL treatment, there was an obvious decrease in the number of total cells and N-cadherin expression (Supplementary Data Fig. S2), preventing observations on the cytopathology of IVH beyond this time. Treatment with 25 or 30 μL of blood permitted long-term experiments since the model offered a sufficient and reliable number of VZ cells even after 48 hours (Supplementary Data Fig. S2; Figs. 2–4) similar to the human condition. On the basis of these findings, 30 μL of blood treatment was used for the remainder of the experiments.

NSC/EC Alterations

To characterize VZ disruption, the total number of cells, the percentage of EC and programed cell death was evaluated over time. After 3 hours of PBS or blood treatment, no differences in the total number of VZ DAPI-positive cells per 0.0225 mm^2 were found (38.62 ± 11.47 vs 42.78 ± 8.614); however, a significant reduction of total VZ cells was observed after 24 hours of blood exposure (41.45 ± 5.62 vs 32.08 ± 10.68; $p < 0.05$) and after 48 hours (44.31 ± 6.87 vs 26.94 ± 7.50; $p < 0.001$) (Fig. 4A, B). A similar effect was found for multiciliated cells, as shown by changes in βIV-tubulin signal; there was no change in multiciliated cells after 3 hours of treatment, but a decrease was noted after 24 hours (control 31.07 ± 7.78 vs IVH 11.84 ± 7.86; $p < 0.001$) and after 48 hours (control 52.29 ± 11.07 vs IVH 14.65 ± 8.49; $p < 0.001$). Interestingly, immunohistochemistry against active caspase 3, a marker of apoptosis, showed no change in caspase 3-positive cells at the same time points (respectively control vs blood; 3 hours: 2.93 ± 0.70 vs 3.39 ± 2.63; 24 hours: 3.72 ± 0.42 vs 2.50 ± 2.80; 48 hours: 3.19 ± 1.00 vs 1.823 ± 1.16), suggesting that programmed cell death was not a factor in cell loss following blood exposure (Fig. 2D; Supplementary Data Fig. S2B). We then calculated the percentage

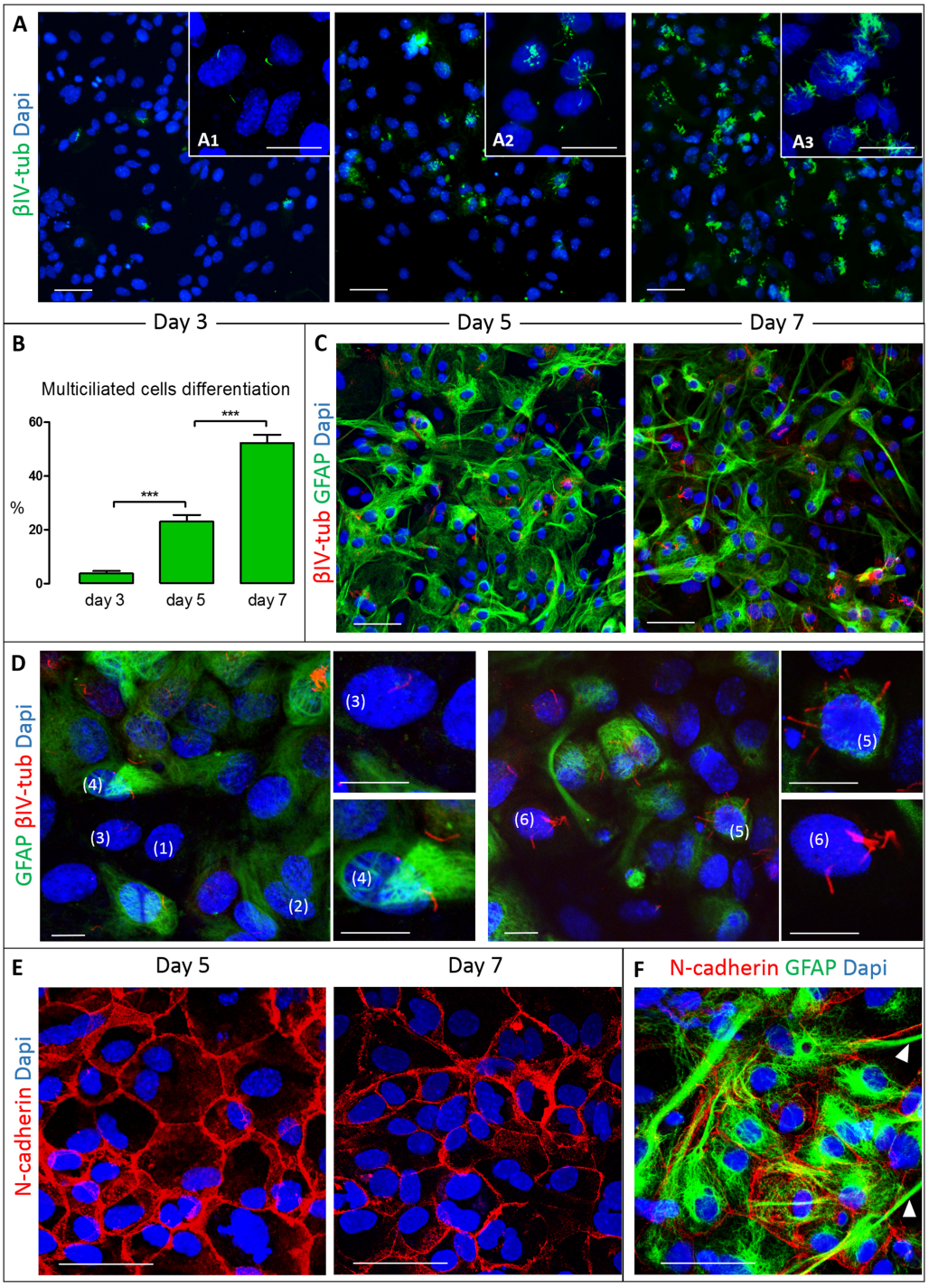

FIGURE 1. VZ cell culture used for the in vitro blood exposure model. Representative images of VZ cells at different stages of differentiation and maturation. **(A)** VZ cells undergo differentiation into multiciliated EC from day 3 to day 7, identified using cilia marker βIV tubulin (images acquired at 20×). Insets **A1**, **A2**, and **A3** show representative images of cell cultures at higher power resolution (63×) at days 3, 5, and 7, respectively, detailing monociliated cells that differentiate into multiciliated cells over time. **(B)** The percentage of multiciliated EC progressively increased between days 3, 5, and 7 (***denotes $p < 0.001$ one-way ANOVA with Tukey posthoc test). **(C)** Expression of GFAP (green) in cultures of multiciliated EC identified by βIV tubulin (red) at day 5 and 7. **(D)** Detail of double-labeling of GFAP and βIV tubulin showing a mixed population of cells, including those not expressing GFAP or βIV tubulin (1), expressing GFAP only (2), GFAP-negative monociliated cells (3), GFAP-positive monociliated cells (4), GFAP-positive multiciliated cells (5), and GFAP-negative multiciliated cells (6). **(E)** N-cadherin-based cell-cell junctions, with characteristic membrane signal location and polygonal morphology at day 5 and 7. **(F)** Expression of N-cadherin (red) and GFAP (green) showing that the glial projections do not colocalize with cell-cell junctions (arrowheads). Scale bars: **A, C, E, F** = 50 μm; **A1, A2, A3** = 20 μm; **D** = 10 μm.

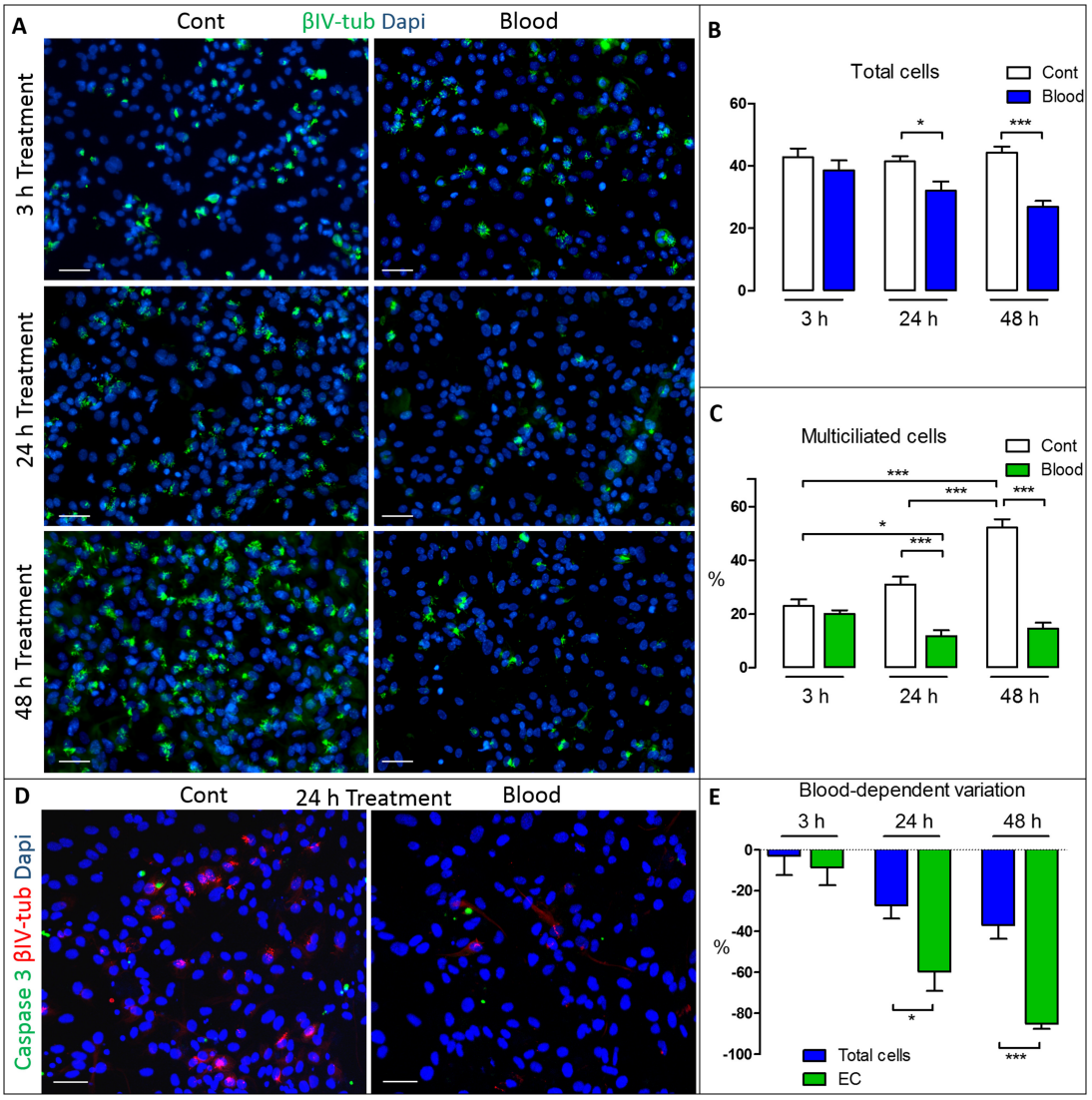

FIGURE 2. Time-dependent effect of blood in VZ cell cultures. After 5 days of differentiation samples were analyzed at 3, 24, and 48 hours of control (Cont) or blood exposure. Controls exhibit normal differentiation from NSC to ependymal cells **(A, C)**, with significant increases in the percentage of βIV-tubulin multiciliated cells **(C)**. Blood exposure significantly reduces both the total number of cells (DAPI-positive cells/0.0225 mm^2) **(B)** and the percentage of multiciliated cells at 24 hours and 48 hours **(C)**. *$p < 0.05$; **$p < 0.01$; ***$p < 0.001$. **(D)** Double-labeling with active caspase 3 (green) and βIV-tubulin (red) showed no difference in the number of apoptotic cells. **(E)** Blood exposure-dependent proportional change of total cells versus ependymal cells (EC). EC decrease was twice as high after 24 hours and even greater after 48 hours than the cell loss, showing a significant discrepancy between total cell loss and the lack of EC. *$p < 0.05$; ***$p < 0.001$; Student *t*-test was used to analyze the total cells **(B)** and the blood-dependent variation **(E)**; one-way ANOVA and a Tukey posthoc test were used to analyze the mean percentage of ciliated cells **(C)**. Scale bars: 50 μm in all panels.

of total cell loss (loss of DAPI-positive cells) after blood and compared it with the percentage of EC diminution (diminution of multiciliated βIV-tubulin-positive cells) at 3, 24, and 48 hours of blood treatment. After 3 hours there was essentially no discrepancy between total cell loss and EC diminution (respectively, -2.92 ± 28.72 vs -8.60 ± 24.84); however, after 24 hours EC diminution was twice as high as total cell loss (respectively, $-59.68\% \pm 25.10\%$ vs $-27.12\% \pm 21.94\%$; $p < 0.05$) and even greater after 48 hours (respectively, $-85.16\% \pm 9.15\%$ vs $-36.90\% \pm 23.98\%$; $p < 0.001$) (Fig. 2E). These results demonstrated that the EC loss exceeded total cell loss and suggest that cell loss is not the sole factor in the decrease of the multiciliated EC after blood treatment. Indeed, other factors, such as alterations in NSC/EC differentiation, may contribute to the diminution in EC following blood exposure.

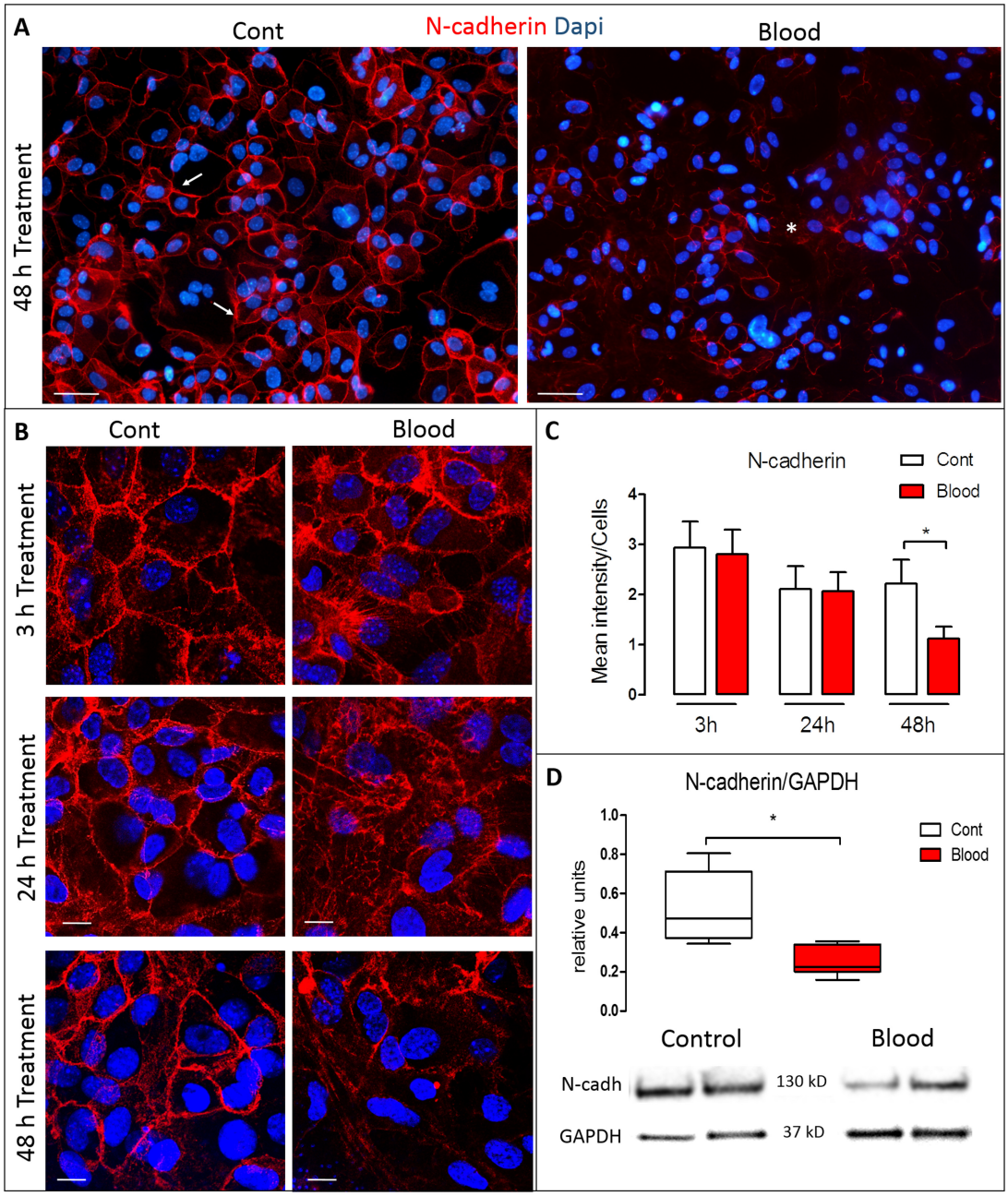

FIGURE 3. Time-dependent effect of blood in N-cadherin expression in the VZ. **(A)** Representative VZ cultures after 48 hours of control (left) or blood exposure (right). Compared with the prominent expression of N-cadherin (red) at the cell membrane in controls (arrows), N-cadherin expression was weaker and cytoplasmically dislocated after blood exposure (asterisk). **(B)** High magnification of VZ N-cadherin labeling in which 3 hours after exposure to blood, no changes were found in the expression of N-cadherin (red). However, after 24 hours of treatment, the expression of N-cadherin fragmented, with loss of the lattice-like configuration. After 48 hours, there was fragmentation, dislocation from the cell membrane, and loss of N-cadherin expression. **(C)** Quantification and comparison of N-cadherin expression between control and blood exposure, normalized by the total number of cells. There was a significant decrease in N-cadherin expression after 48 hours of blood treatment ($p < 0.05$). **(D)** N-cadherin protein levels quantified by Western blot normalized by GAPDH showing decreased levels of N-cadherin after 48 hours of blood treatment. Data are mean of the immunodensity/cells from 2 experiments with at least $n = 6$ wells at 3, 24, and 48 hours, respectively **(C)**, and protein levels (N-cadherin/GAPDH) by Western blot (*$p < 0.05$) Data were analyzed from 2 experiments with $n = 4$ per condition **(D)**. Nonparametric Mann-Whitney *U* test was used to analyze the data. Scale bars: All **A** panels = 50 μm; all **B** panels = 10 μm.

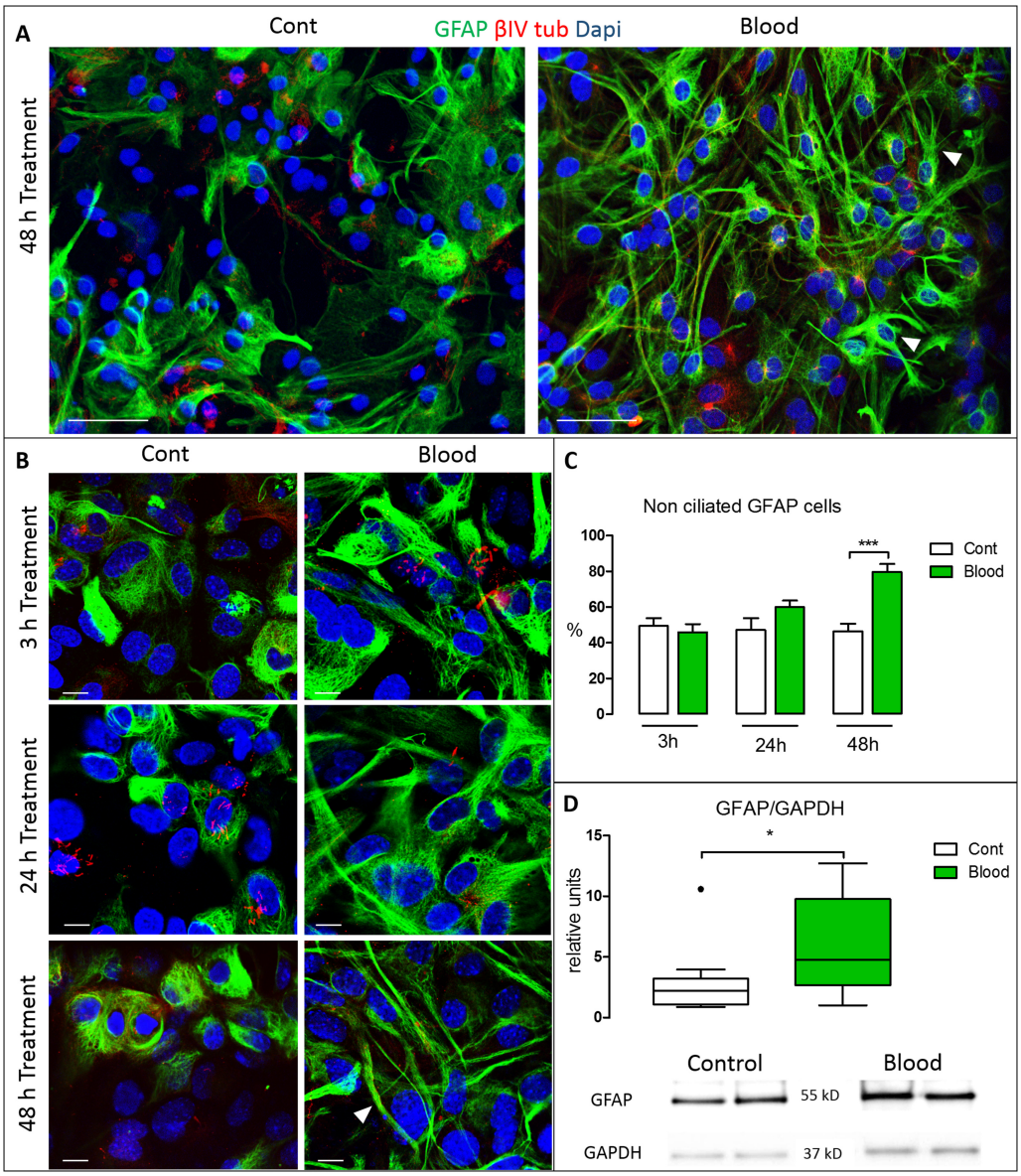

FIGURE 4. Glial activation in the VZ. **(A)** Representative VZ culture immunostained after 48 hours of blood treatment illustrating the appearance of GFAP-positive cells (arrowheads). **(B)** High-resolution images of cells double-labeled with βIV-tubulin and GFAP antibodies after 3, 24, and 48 hours of blood treatment versus control. After 48 hours treatment, most GFAP-positive cells exhibited numerous long, thin projections (arrowhead), typical of reactive astrocytes. **(C)** Quantification of nonciliated GFAP-positive cells. After 48 hours treatment the mean number of cells expressing GFAP was significantly increased (***$p < 0.001$; Student *t*-test). **(D)** GFAP protein levels quantified by Western blot normalized by GAPDH showing increased levels of GFAP after 48 hours of blood treatment (*$p < 0.05$; nonparametric Mann-Whitney *U* test). Scale bars: All **A** panels = 50 μm; all **B** panels = 10 μm.

Cell Junction Pathology

To gain insight into contributing factors in VZ disruption after blood exposure, the integrity of the cell-cell junctions was examined using N-cadherin expression. After 3 hours of blood exposure, no changes were found in the expression of N-cadherin (control: 2.29 ± 2.40, blood: 2.76 ± 2.37). After 24 hours of blood treatment, the N-cadherin signal profile became fragmented, with loss of the typical lattice-like cell membrane expression and a prevalence of abnormal subcellular cytosolic depositions (Fig. 3A, B); however, the total amount of N-cadherin was not significantly different when immuno-density was quantified (control: 2.11 ± 2.03, blood: 2.06 ± 2.10). After 48 hours of blood treatment, the abnormal deposition and fragmentation persisted, as well as a significant loss of N-cadherin signal (control: 2.21 ± 1.87, blood: 1.12 ± 1.07; $p < 0.05$; Fig. 3A–C). Significant reduction of N-cadherin signal was confirmed with

Western blots by measuring the N-cadherin/GAPDH ratio (median of control vs blood 0.47 ± 0.17, 0.22 ± 0.03, $p < 0.05$) after 48 hours of blood treatment (Fig. 3D).

Glial Activation

GFAP immunolabeling was also employed to investigate astroglial differentiation following blood exposure. The percentage of nonciliated GFAP-positive cells did not change after 3 hours (control 49.44 ± 12.96 vs blood 45.94 ± 16.33) or 24 hours (control 47.16 ± 17.33 vs blood 59.94 ± 13.53) but increased significantly after 48 hours of blood treatment; (control vs blood, respectively, 47.10 ± 13.21, 79.63 ± 11.81; $p < 0.05$; Fig. 4A, B). Morphological changes were also observed in GFAP-expressing cells from 3 to 48 hours of blood exposure. In particular, GFAP-positive cells exhibited branch-like projections and a larger GFAP-positive cytoskeleton; at 48 hours, the GFAP-positive processes appeared elongated (Fig. 4A, B) consistent with reactive astrocytes. These findings were further supported by the fact that the cells treated with blood for 48 hours presented increased levels of the GFAP/GAPDH ratio when measured by Western blot (median of control vs blood 1.99 ± 1.01, 4.75 ± 4.1, $p < 0.05$) (Fig. 4D).

DISCUSSION

The pathogenesis of PHH remains poorly understood (8, 9), in part due to a lack of tools enabling molecular studies on the pathophysiology of PHH. As a first step in this work we developed an in vitro model of ventricular hemorrhage to determine if blood causes VZ disruption and glial activation. Our results suggest that blood impairs N-cadherin-dependent cell junctions and results in loss of multiciliated cells, and subsequently glial activation, closely mimicking the events reported in humans and in animal models of fetal-onset congenital and posthemorrhagic hydrocephalus (10, 18, 19, 22–26, 28, 29, 31, 38).

This murine in vitro model of IVH injury sought to mimic the normal cell differentiation in the VZ of the preterm infant. In rats, the differentiation of the dorsolateral wall of the lateral ventricle takes place postnatally. At postnatal day 1 is formed by ~70% of NSC, ~23% of nonciliated cells, and ~7% multiciliated EC. From this time onward, the NSC differentiate into multiciliated EC; nevertheless, the percentage of nonciliated cells remains constant throughout VZ development (31). A similar pattern of postnatal ependymal maturation has been found in mice (33); however, in humans the maturation of EC occurs earlier in intrauterine life. Humans present multiciliated EC in the dorsolateral wall from 23 to 40 gestational weeks (10, 31, 39). To model the clinical timeline of VZ development as closely as possible, our experiments were performed in the stage of differentiation when the cultured cells progress from ~20% to ~55% multiciliated EC between in vitro day 5 and day 7. During this period of time the VZ also exhibited preterm human-like features such as the presence of undifferentiated monociliated cells with or without expression of GFAP, immature multiciliated EC expressing GFAP (~65% of all EC) and mature EC not expressing GFAP (~35%). Since, the presence of monocilia is the main characteristic of NSC (11), and GFAP is a glial cell marker for astrocytes and immature EC, monociliated cells not expressing GFAP may belong to another lineage of stem cells not committed to macroglia.

Cell junction pathobiology may mediate the VZ disruption in clinical and experimental hydrocephalus (18, 19, 23, 38, 40–44). In areas of VZ disruption, N-cadherin is located within the cytoplasm rather than bound to the cell membrane (31). Furthermore, many genetic alterations that directly or indirectly alter the stability of cell junctions are associated with VZ disruption and the development of hydrocephalus (29, 38, 45–47). The blood component lysophosphatidic acid has also been shown to alter cell junctions, disrupt the cytoarchitecture of the VZ, and produce hydrocephalus (22, 25). It is worth noting that these authors found VZ disruptions in both the lateral ventricles and the cerebral aqueduct, and therefore suggested that acqueductal stenosis was involved in producing ventriculomegaly in their rodent model. Our IVH in vitro model is also consistent with these well-known cell junction alterations since dislocations of N-cadherin were found after 24 hours of blood treatment and significantly decreased expression of N-cadherin was seen after 48 hours of treatment. Attachment of VZ cells are mediated by adherens junctions, therefore impairment of these junctions result in detachment and loss of those cells. Since cell junctions appear to be fundamental to the genesis of cytopathology in many forms of hydrocephalus, modulators of those molecules should be playing a role in the etiology of this disease. A disintegrin and metalloproteinase domain-containing protein 10 (ADAM10) is a metalloproteinase responsible of the cleavage of >40 transmembrane proteins in the extracellular region (48); most of these are cell adhesion proteins such as L1-CAM (49) and E- and N-cadherin (reviewed in (50)) and its activation produces disruption of epithelial cells of the lung in mice by cleaving E-cadherin (51) presenting a pattern of cadherin disruption similar to what we have observed in our in vitro model. Interestingly, we reported previously that many of the proteins cleaved by ADAM10 such as amyloid precursor protein and L1-CAM have been found to be increased in the CSF of both congenital and posthemorrhagic hydrocephalus (52–55). Since ADAM10 plays a key role in the biology of cell adhesion, future studies on this molecule are warranted to determine its role in the pathogenesis of hydrocephalus.

The IVH in vitro model also resulted in fewer total VZ cells after 24 hours of treatment, possibly due to loss of adherens junctions. Interestingly, there were fewer multiciliated cells at 24 and 48 hours, which suggests that those cells may be more affected by this detachment; however, the percentage of VZ cell loss is not proportional to the percentage of the diminution of EC. We found that the decrease of EC is 2 times greater than the cell loss indicating that cell loss is not the only factor involved in the lack of EC. Also, an impairment in the differentiation of the EC seem to be taking place, probably due to the aforementioned blood-dependent N-cadherin effects. This is consistent with the findings reported by Muniz-Talavera and Schmidt where mutant mice lacking the junctional cadherin complex regulator (Jhy) showed protracted differentiation of the EC and hydrocephalus (56). In

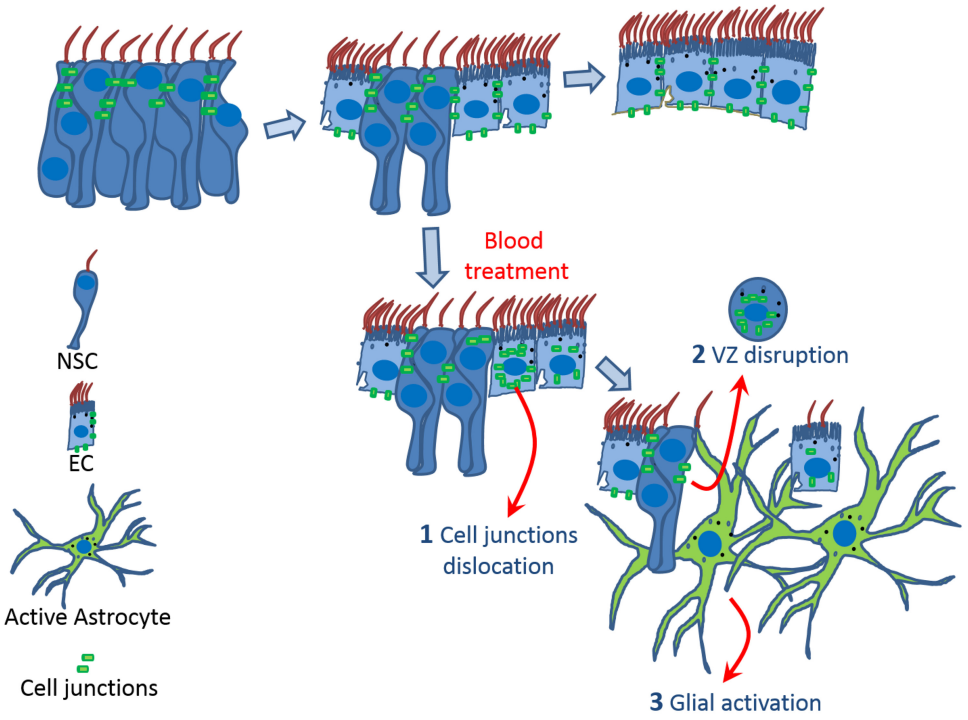

FIGURE 5. Model summarizing the effects of the blood on the VZ. During maturation **(A–C)**, neural stem cells (NSC) with adherens junctions transform into multiciliated ependymal cells (EC). Blood exposure produces a time-dependent chain of events starting with the dislocation of cell junctions (N-cadherin) from the cell membrane into the cytoplasm and loss of multiciliated cells. Subsequently, glial activation occurs, as evidenced by astrocytes with numerous processes. In vivo observations suggest that glial activation occurs at the site of VZ disruption.

both human and animal cases, the VZ disruption is linked to a glial activation, possibly forming a new layer that specifically repairs, or "patches," the disrupted area (23, 26, 57). This experimental model is consistent with this theory, displaying a significant increase in the number of cells expressing GFAP at 48 hours and exhibiting multiple projections reminiscent of a reactive astroglial response. This glial response occurred 24 hours after disruption of N-cadherin and the loss of multiciliated cells was detected, indicating that this reaction may respond to the impairment in the cell junctions and the VZ cell loss. These alterations seem to be promoting NSC, originally committed to become EC, to differentiate into reactive astrocytes, thus changing the VZ program of differentiation which would also explain the discrepancy found between cell loss and EC differentiation. This glial activation, especially the addition of branched processes, influences the overall decrease of N-cadherin levels found after 48 hours of blood treatment since this junction protein is not expressed in the glial projections.

In summary, we showed VZ blood exposure triggers a time-dependent chain of events starting with the dislocation of N-cadherin, an impairment in the differentiation and loss of EC and later on, a glial activation (Fig. 5).

Multiciliated EC are involved in the flow of the CSF adjacent to the VZ and the lack of those multicilia may disrupt ventricular CSF flow associated with hydrocephalus. This is been supported by findings from Appeble et al and Muniz-Talavera and Schmidt (56, 58) in which Jhy knock out mice showed impairments in the development of the multiciliated EC and ventriculomegaly. Interestingly, Jhy is the main junctional cadherin complex regulator; this means that a correlation exists between cadherin regulation and VZ maturation. We have shown that blood exposure disrupted N-cadherin-dependent cell junctions and subsequently the VZ, but the specific blood components responsible for these changes are not known. The serine protease thrombin induces VZ disruption and hydrocephalus (59), as well as the aforementioned LPA (22, 25) affecting the cell junctions. Iron or hemoglobin has also been used in neonatal rats to produce hydrocephalus; however, the mechanisms involved in VZ disruption were not defined (60).

The disruption of the VZ may have other consequences besides changes in CSF flow by ciliary beating. The VZ is the niche of neurogenesis and gliogenesis of the brain in which the NSC proliferate and migrate using the basal projections of neighbor NSC. Therefore, alterations or loss of cells in this zone cause other developmental complications such as an inability to migrate by the loss of the NSC structural scaffold; this results in characteristic periventricular heterotopia formed by neurons unable to migrate (10, 31), or changes in the proportionality of neurons and glial cells in favor of astrocytes. We hypothesize that glial activation linked to VZ disruption in fetal life induces NSC meant to be neurons to become astrocytes. Thus, we support the idea that alterations of the VZ during fetal life by IVH may change the intrinsic structure of the white and gray matter in the brain.

Conclusion

In this in vitro model, blood exposure directly affects the stability of N-cadherin-based cell-cell junctions leading to the disruption of the VZ by cell loss and impairment in the differentiation of the EC, followed by a glial activation. This in vitro model of IVH may be a useful tool to further define these mechanisms and others that contribute to the pathogenesis of this devastating disease.

ACKNOWLEDGMENTS

We thank Dr Wolfgang Pita and Dr Marina Pulido for their invaluable advice in developing this cell culture.

REFERENCES

1. Adams-Chapman I, Hansen NI, Stoll BJ, et al. Neurodevelopmental outcome of extremely low birth weight infants with posthemorrhagic hydrocephalus requiring shunt insertion. Pediatrics 2008;121:e1167–77
2. McCrea HJ, Ment LR. The diagnosis, management, and postnatal prevention of intraventricular hemorrhage in the preterm neonate. (Review) Clin Perinatol 2008;35:777–92, vii
3. Stoll BJ, Hansen NI, Bell EF, et al. Trends in care practices, morbidity, and mortality of extremely preterm neonates, 1993–2012. JAMA 2015; 314:1039–51
4. Christian EA, Jin DL, Attenello F, et al. Trends in hospitalization of preterm infants with intraventricular hemorrhage and hydrocephalus in the United States, 2000–2010. J Neurosurg Pediatr 2016;17:260–9
5. Murphy BP, Inder TE, Rooks V, et al. Posthaemorrhagic ventricular dilatation in the premature infant: Natural history and predictors of outcome. Arch Dis Child Fetal Neonatal Ed 2002;87:F37–41
6. Vassilyadi M, Tataryn Z, Shamji MF, et al. Functional outcomes among premature infants with intraventricular hemorrhage. Pediatr Neurosurg 2009;45:247–55
7. Limbrick DD, Jr., Mathur A, Johnston JM, et al. Neurosurgical treatment of progressive posthemorrhagic ventricular dilation in preterm infants: A 10-year single-institution study. J Neurosurg Pediatr 2010;6:224–30
8. Strahle J, Garton HJ, Maher CO, et al. Mechanisms of hydrocephalus after neonatal and adult intraventricular hemorrhage. Transl Stroke Res 2012;3:25–38
9. Garton T, Keep RF, Wilkinson DA, et al. Intraventricular hemorrhage: The role of blood components in secondary injury and hydrocephalus. Transl Stroke Res 2016;7:447–51
10. McAllister JP, Guerra MM, Ruiz LC, et al. Ventricular zone disruption in human neonates with intraventricular hemorrhage. J Neuropathol Exp Neurol 2017;76:358–75
11. Kriegstein A, Alvarez-Buylla A. The glial nature of embryonic and adult neural stem cells. Annu Rev Neurosci 2009;32:149–84
12. Bayatti N, Moss JA, Sun L, et al. A molecular neuroanatomical study of the developing human neocortex from 8 to 17 postconceptional weeks revealing the early differentiation of the subplate and subventricular zone. Cereb Cortex 2008;18:1536–48
13. Bystron I, Blakemore C, Rakic P. Development of the human cerebral cortex: Boulder Committee revisited. Nat Rev Neurosci 2008;9:110–22
14. De Juan Romero C, Borrell V. Coevolution of radial glial cells and the cerebral cortex. Glia 2015;63:1303–19
15. Rowitch DH, Kriegstein AR. Developmental genetics of vertebrate glial-cell specification. Nature 2010;468:214–22
16. Molofsky AV, Krencik R, Ullian EM, et al. Astrocytes and disease: A neurodevelopmental perspective. Genes Dev 2012;26:891–907
17. Malik S, Vinukonda G, Vose LR, et al. Neurogenesis continues in the third trimester of pregnancy and is suppressed by premature birth. J Neurosci 2013;33:411–23
18. Paez P, Batiz LF, Roales-Bujan R, et al. Patterned neuropathologic events occurring in hyh congenital hydrocephalic mutant mice. J Neuropathol Exp Neurol 2007;66:1082–92
19. Jimenez AJ, Garcia-Verdugo JM, Gonzalez CA, et al. Disruption of the neurogenic niche in the subventricular zone of postnatal hydrocephalic hyh mice. J Neuropathol Exp Neurol 2009;68:1006–20
20. Tissir F, Qu Y, Montcouquiol M, et al. Lack of cadherins Celsr2 and Celsr3 impairs ependymal ciliogenesis, leading to fatal hydrocephalus. Nat Neurosci 2010;13:700–7
21. Wilson GR, Wang HX, Egan GF, et al. Deletion of the Parkin co-regulated gene causes defects in ependymal ciliary motility and hydrocephalus in the quakingviable mutant mouse. Hum Mol Genet 2010;19: 1593–602
22. Yung YC, Mutoh T, Lin ME, et al. Lysophosphatidic acid signaling may initiate fetal hydrocephalus. Sci Transl Med 2011;3:99ra87
23. Roales-Bujan R, Paez P, Guerra M, et al. Astrocytes acquire morphological and functional characteristics of ependymal cells following disruption of ependyma in hydrocephalus. Acta Neuropathol 2012;124: 531–46
24. Rodriguez EM, Guerra MM, Vio K, et al. A cell junction pathology of neural stem cells leads to abnormal neurogenesis and hydrocephalus. Biol Res 2012;45:231–42
25. Park R, Moon UY, Park JY, et al. Yap is required for ependymal integrity and is suppressed in LPA-induced hydrocephalus. Nat Commun 2016;7: 10329
26. Fukumizu M, Takashima S, Becker LE. Glial reaction in periventricular areas of the brainstem in fetal and neonatal posthemorrhagic hydrocephalus and congenital hydrocephalus. Brain Dev 1996;18:40–5
27. Fukumizu M, Takashima S, Becker LE. Neonatal posthemorrhagic hydrocephalus: Neuropathologic and immunohistochemical studies. Pediatr Neurol 1995;13:230–4
28. Dominguez-Pinos MD, Paez P, Jimenez AJ, et al. Ependymal denudation and alterations of the subventricular zone occur in human fetuses with a moderate communicating hydrocephalus. J Neuropathol Exp Neurol 2005;64:595–604
29. Sival DA, Guerra M, den Dunnen WF, et al. Neuroependymal denudation is in progress in full-term human foetal spina bifida aperta. Brain Pathol 2011;21:163–79
30. Acabchuk RL, Sun Y, Wolferz R, Jr, 3D modeling of the lateral ventricles and histological characterization of periventricular tissue in humans and mouse. J Vis Exp 2015;99
31. Guerra MM, Henzi R, Ortloff A, et al. Cell junction pathology of neural stem cells is associated with ventricular zone disruption, hydrocephalus, and abnormal neurogenesis. J Neuropathol Exp Neurol 2015;74: 653–71
32. Yamamoto H, Maruo T, Majima T, et al. Genetic deletion of afadin causes hydrocephalus by destruction of adherens junctions in radial glial and ependymal cells in the midbrain. PLoS One 2013;8:e80356
33. Delgehyr N, Meunier A, Faucourt M, et al. Ependymal cell differentiation, from monociliated to multiciliated cells. Methods Cell Biol 2015; 127:19–35
34. Hoff J. Methods of Blood Collection in the Mouse. 2000
35. Roessmann U, Velasco ME, Sindely SD, et al. Glial fibrillary acidic protein (GFAP) in ependymal cells during development. An immunocytochemical study. Brain Res 1980;200:13–21
36. Bruni JE, Del Bigio MR, Clattenburg RE. Ependyma: Normal and pathological. A review of the literature. Brain Res Rev 1985;9:1–19
37. Sarnat HB. Regional differentiation of the human fetal ependyma: Immunocytochemical markers. J Neuropathol Exp Neurol 1992;51:58–75
38. Batiz LF, Paez P, Jimenez AJ, et al. Heterogeneous expression of hydrocephalic phenotype in the hyh mice carrying a point mutation in alpha-SNAP. Neurobiol Dis 2006;23:152–68
39. Gould SJ, Howard S, Papadaki L. The development of ependyma in the human fetal brain: An immunohistological and electron microscopic study. Brain Res Dev Brain Res 1990;55:255–67
40. Perez-Figares JM, Jimenez AJ, Perez-Martin M, et al. Spontaneous congenital hydrocephalus in the mutant mouse hyh. Changes in the ventricular system and the subcommissural organ. J Neuropathol Exp Neurol 1998;57:201–2
41. Jimenez AJ, Tome M, Paez P, et al. A programmed ependymal denudation precedes congenital hydrocephalus in the hyh mutant mouse. J Neuropathol Exp Neurol 2001;60:1105–19
42. Wagner C, Batiz LF, Rodriguez S, et al. Cellular mechanisms involved in the stenosis and obliteration of the cerebral aqueduct of hyh mutant mice developing congenital hydrocephalus. J Neuropathol Exp Neurol 2003;62:1019–40
43. Batiz LF, Jimenez AJ, Guerra M, et al. New ependymal cells are born postnatally in two discrete regions of the mouse brain and support

ventricular enlargement in hydrocephalus. Acta Neuropathol 2011;121: 721–35
44. Feldner A, Adam MG, Tetzlaff F, et al. Loss of Mpdz impairs ependymal cell integrity leading to perinatal-onset hydrocephalus in mice. EMBO Mol Med 2017;9:890–905
45. Klezovitch O, Fernandez TE, Tapscott SJ, et al. Loss of cell polarity causes severe brain dysplasia in Lgl1 knockout mice. Genes Dev 2004; 18:559–71
46. Rasin MR, Gazula VR, Breunig JJ, et al. Numb and Numbl are required for maintenance of cadherin-based adhesion and polarity of neural progenitors. Nat Neurosci 2007;10:819–27
47. Ferland RJ, Batiz LF, Neal J, et al. Disruption of neural progenitors along the ventricular and subventricular zones in periventricular heterotopia. Hum Mol Genet 2009;18:497–516
48. Jouannet S, Saint-Pol J, Fernandez L, et al. TspanC8 tetraspanins differentially regulate the cleavage of ADAM10 substrates, Notch activation and ADAM10 membrane compartmentalization. Cell Mol Life Sci 2016; 73:1895–915
49. Mechtersheimer S, Gutwein P, Agmon-Levin N, et al. Ectodomain shedding of L1 adhesion molecule promotes cell migration by autocrine binding to integrins. J Cell Biol 2001;155:661–73
50. Saftig P, Reiss K. The "A Disintegrin And Metalloproteases" ADAM10 and ADAM17: Novel drug targets with therapeutic potential? Eur J Cell Biol 2011;90:527–35
51. Inoshima I, Inoshima N, Wilke GA, et al. A Staphylococcus *aureus* pore-forming toxin subverts the activity of ADAM10 to cause lethal infection in mice. Nat Med 2011;17:1310–4
52. Morales DM, Townsend RR, Malone JP, et al. Alterations in protein regulators of neurodevelopment in the cerebrospinal fluid of infants with posthemorrhagic hydrocephalus of prematurity. Mol Cell Proteomics 2012;11:M111.011973
53. Limbrick DD, Jr, Baksh B, Morgan CD, et al. Cerebrospinal fluid biomarkers of infantile congenital hydrocephalus. PLoS One 2017;12: e0172353
54. Limbrick DD, Jr, Castaneyra-Ruiz L, Han RH, et al. Cerebrospinal fluid biomarkers of pediatric hydrocephalus. Pediatric Neurosurg 2017;52: 426–35
55. Morales DM, Silver SA, Morgan CD, et al. Lumbar cerebrospinal fluid biomarkers of posthemorrhagic hydrocephalus of prematurity: Amyloid precursor protein, soluble amyloid precursor protein alpha, and L1 cell adhesion molecule. Neurosurgery 2017;80:82–90
56. Muniz-Talavera H, Schmidt JV. The mouse Jhy gene regulates ependymal cell differentiation and ciliogenesis. PLoS One 2017;12:e0184957
57. Jimenez AJ, Dominguez-Pinos MD, Guerra MM, et al. Structure and function of the ependymal barrier and diseases associated with ependyma disruption. Tissue Barriers 2014;2:e28426
58. Appelbe OK, Bollman B, Attarwala A, et al. Disruption of the mouse Jhy gene causes abnormal ciliary microtubule patterning and juvenile hydrocephalus. Dev Biol 2013;382:172–85
59. Gao F, Liu F, Chen Z, et al. Hydrocephalus after intraventricular hemorrhage: The role of thrombin. J Cereb Blood Flow Metab 2014;34:489–94
60. Strahle JM, Garton T, Bazzi AA, et al. Role of hemoglobin and iron in hydrocephalus after neonatal intraventricular hemorrhage. Neurosurgery 2014;75:696–705;discussion 6